*The Monte Carlo Method: Versatility Unbounded In A Dynamic Computing World*
Chattanooga, Tennessee, April 17–21, 2005, on CD-ROM, American Nuclear Society, LaGrange Park, IL (2005)

# MONTE CARLO SIMULATION OF ELECTRONS BACKSCATTERED FROM SURFACE CARBON FILMS

**Maurizio Dapor**
IRST
I-38050 Povo, Trento, Italy
dapor@itc.it

## ABSTRACT

We have computed, by a Monte Carlo code, the backscattering coefficient of low-medium energy electron beams (from 250 eV to 10,000 eV) impinging on carbon films deposited on two different substrates (Al and Cu). Investigating the behaviour of the backscattering coefficient as a function of the primary energy for various surface film thicknesses, we have found an interesting property, i.e. the appearance of relative maxima of absorption (and relative minima of backscattering).

A characteristic of the relative minima is that their position shifts towards higher energies, while the peaks are broadening, as the film thickness increases.

The trend presented can be used as a way to measure the carbon film thickness by a set of measures of the backscattering coefficient.

*Key Words*: Backscattering coefficient, surface films, Monte Carlo simulation

## 1 INTRODUCTION

When an electron-beam impinges on a solid target, each individual electron loses energy and changes its direction of motion due to atomic electron excitation, plasmon emission and interactions with the nuclei of the medium.

The travel of the electron in the solid may be described by means of the inelastic scattering processes due to the interaction between the incident electrons and the atomic electrons, and the elastic scattering processes due to the collisions between the incident electrons and the nuclei.

Once calculated the electron inelastic and elastic scattering cross sections, it is possible to deal with the problem of the interaction of an electron-beam with a solid by using the Monte Carlo method.

This work is focused on the simulation of the interaction of an electron-beam with solid targets constituted by thin films of C deposited on two different substrates: Al and Cu.

There are a lot of technological uses of the films of carbon, as carbon characteristics are very useful in many fields. Carbon films deposited on polymeric substrates can be used to replace the metallic coatings on plastic materials used for food package. Carbon-based coatings allow plastics to be recycled and today several researchers are looking for carbon films for food package impermeable to atmospheric gases, transparent to visible light, and mechanically stable. Carbon films are also widely employed in medical devices. Biomedical investigators have demonstrated that permanent thin films of pure carbon show an excellent

haemo/biocompatibility: they are used, in particular, as coating for the stainless steel stents to be implanted in coronary arteries.

The study of carbon films is thus important for many applications, and this paper reports the results of a Monte Carlo simulation of the backscattering coefficient of low-medium energy electron beams (from 250 eV to 10,000 eV) impinging on carbon films of various thicknesses deposited on two different substrates.

## 2 METHODS

In order to describe the processes which occur when an electron beam penetrates in a solid target, we need to know the elastic and the inelastic collisions suffered by the electrons traveling in the solid. Indeed, in each collision event with an atomic electron or a nucleus, the incident electrons both loses energy and changes its traveling direction. The energy dissipation of the incident electron mainly occurs through atomic electron excitation or ejection and plasmon excitation. These scattering processes also influence the electron trajectory in the solid, but only weakly. The nuclear collisions, on the other hand, due to the large mass difference between the electron and the atomic nucleus, are nearly elastic: they strongly affect the direction of the incident electron without substantial energy transfer.

The differential elastic-scattering cross section calculation of electrons interacting with free and bound atoms, in particular for low-medium kinetic energy, requires numerical quantum-mechanical calculation. The inelastic events can be described, in the continuous slowing down approximation, by the stopping power, viz., the mean energy loss per unit distance traveled by the electron inside the solid.

### 2.1 Elastic Scattering: the Relativistic Partial Wave Expansion Method (RPWEM)

The elastic scattering process can be treated by calculating the phase shifs. Since the large-radial coordinate asymptotic behavior of the radial wave function is known, the phase shifts can be computed by solving the Dirac's equation for a central electrostatic field up to a large radius for which the atomic potential can be safely ignored (Relativistic Partial Wave Expansion Method, RPWEM in the following). The details of the calculation, which are here briefly summarized, can be found in the references [1-3].

Using the natural units $\hbar=c=1$, the Dirac equation describing an electron in the presence of a central electrostatic field can be written as

$$\frac{d\phi_l^{\pm}(r)}{dr} = \frac{k}{r}\sin 2\phi_l^{\pm}(r) - m\cos 2\phi_l^{\pm}(r) + E - V(r), \tag{1}$$

where

$$k = \begin{cases} -(l+1) & \text{spin up}: \phi_l^{+}(r) \\ l & \text{spin down}: \phi_l^{-}(r) \end{cases}, \tag{2}$$

$l$=1,2,…∞, $m$ is the electron mass, $E$ the electron kinetic energy, $V(r)$ the central electrostatic potential energy and $r$ the radial coordinate.

Once solved the Dirac equation, one is interested in the calculation of the quantity

$$\widetilde{\phi}_l^{\pm} = \lim_{r\to\infty} \phi_l^{\pm}(r). \tag{3}$$

In other words, one is interested in solving the Dirac equation for a central electrostatic field up to a radius where the atomic potential can be safely neglected (typically ~2Å). Indeed, once known the large-*r* asymptotic behaviour of the radial wave function, the phase shifts $\eta_l^{\pm}$ can be computed by using the following equation:

$$\tan\eta_l^{\pm} = \frac{Kj_{l+1}(Kr) - j_l(Kr)\left[(E+m)\tan\widetilde{\phi}_l^{\pm} + (1+l+k)/r\right]}{Kn_{l+1}(Kr) - n_l(Kr)\left[(E+m)\tan\widetilde{\phi}_l^{\pm} + (1+l+k)/r\right]}, \tag{4}$$

where $K$ is the momentum of the electron, $K^2=E^2-m^2$, $j_l$ are the regular-spherical Bessel functions and $n_l$ the irregular-spherical Bessel functions. Let us introduce now the two functions $A_l$ and $B_l$ defined by

$$A_l = \frac{1}{2iK}\left\{(l+1)\left[\exp\left(2i\eta_l^-\right)-1\right] + l\left[\exp\left(2i\eta_l^+\right)-1\right]\right\}, \tag{5}$$

$$B_l = \frac{1}{2iK}\left[\exp\left(2i\eta_l^+\right) - \exp\left(2i\eta_l^-\right)\right]. \tag{6}$$

These functions allow us to calculate the scattering amplitudes $f(\theta)$ and $g(\theta)$:

$$f(\theta) = \sum_{l=0}^{\infty} A_l P_l(\cos\theta), \tag{7}$$

$$g(\theta) = \sum_{l=0}^{\infty} B_l P_l^1(\cos\theta), \tag{8}$$

where $P_l$ are the Legendre polynomials while $P_l^1$ are the associated Legendre functions. The knowledge of the scattering amplitudes allows one to calculate the Sherman function $S(\theta)$:

$$S(\theta) = i\frac{fg^* - f^*g}{|f|^2 + |g|^2} \tag{9}$$

and the differential elastic scattering cross-section $\frac{d\sigma}{d\Omega}$:

$$\frac{d\sigma}{d\Omega} = \left(|f|^2 + |g|^2\right)\left[1 + iS(\theta)\mathbf{P}\cdot\hat{\mathbf{n}}\right]. \tag{10}$$

Note that, in the last equation, $\mathbf{P}$ is the initial polarization vector of the electron beam while $\hat{\mathbf{n}}$ is the unit vector perpendicular to the plane of scattering.

If the beam is completely unpolarized, then $P$=0 and, as a consequence,

$$\frac{d\sigma}{d\Omega} = |f|^2 + |g|^2. \tag{11}$$

Once the differential elastic scattering cross-section is known, the total elastic scattering cross-section $\sigma_{el}$ and the first transport elastic scattering cross-section $\sigma_{tr}$ may be calculated by:

$$\sigma_{el} = \int \frac{d\sigma}{d\Omega} d\Omega , \tag{12}$$

$$\sigma_{tr} = \int (1 - \cos\theta) \frac{d\sigma}{d\Omega} d\Omega . \tag{13}$$

The set of equations collected in this section briefly describes the quantum-relativistic approach to the calculation of the differential, total and transport elastic scattering cross-section.

The atomic potential used for the elastic scattering calculation is the Dirac-Hartree-Fock-Slater for atomic numbers greater than 18. For atomic numbers lower than 19 we used the Hartree-Fock field which is preferable for low-atomic numbers because the non-relativistic fields are realistic where the relativistic effects are small and the LS angular momentum coupling is adequate. Since electrons are identical particles, we have taken into account of the exchange when low-energy elastic scattering was treated: indeed, the incident electron may be captured by an atom with emission of a new electron. When the target atom is bound in a solid, the outer electronic orbitals of the atom are modified. In order to take into account such a change, solid-state effects have to be introduced. To describe solid-state effects, the muffin-tin model has been used in which the potential of each atom of the solid is altered by the nearest-neighbor atoms.

## 2.2 Inelastic Scattering

An electron can lose al large amount of its energy in a single collision: nevertheless the continuous-slowing-down approximation is often used. In this approximation the electron is assumed to continuously dissipate its energy during its travel inside the solids. Thus we need to express the rate of energy lost due to electron-electron and electron-plasmon collisions. As the continuous-slowing down approximation neglects the fluctuations of the energy-loss around its mean value, the energy-loss distribution is often included in the Monte Carlo simulations by the energy straggling parameters.

The inelastic mean free path $\lambda_{inel}$ and the stopping power $\frac{dE}{dl}$ are given, respectively, by

$$\lambda_{inel} = \left[ \int p(E, \hbar\omega) d\hbar\omega \right]^{-1}, \tag{14}$$

$$-\frac{dE}{dl} = \int \hbar\omega p(E, \hbar\omega) d\hbar\omega, \tag{15}$$

with integrations extended over all the allowed values of the energy transfer $\hbar\omega$. Here $p(E, \hbar\omega)$ is the probability for energy loss $\hbar\omega$ per unit distance traveled by an electron of energy $E$. If $q$ is the momentum transfer and $\varepsilon(q, \hbar\omega)$ is the complex dielectric function describing the response of the medium , then $p(E, \hbar\omega)$ is given by

$$p(E, \hbar\omega) = \frac{me^2}{\pi\hbar^2 E} \int_{K_1}^{K_2} \frac{dq}{q} \mathrm{Im}\left[ \frac{-1}{\varepsilon(q, \hbar\omega)} \right], \tag{16}$$

where

$$K_1 = \frac{2m}{\hbar}\left(\sqrt{E} - \sqrt{E-\hbar\omega}\right), \tag{17}$$

and

$$K_2 = \frac{2m}{\hbar}\left(\sqrt{E} + \sqrt{E-\hbar\omega}\right). \tag{18}$$

Using the above theory, Ashley [4] has shown that the stopping power can be well approximated by

$$-\frac{dE}{dl} = \frac{me^2}{\pi\hbar^2 E}\int_0^{E/2} \mathrm{Im}\left[\frac{-1}{\varepsilon(0,\hbar\omega)}\right] G\left(\frac{\hbar\omega}{E}\right)\hbar\omega d(\hbar\omega), \tag{19}$$

where

$$G(x) = \ln\left(\frac{1.166}{x}\right) - \frac{3}{4}x - \frac{x}{4}\ln\left(\frac{4}{x}\right) + \frac{1}{2}x^{3/2} - \frac{x^2}{16}\ln\left(\frac{4}{x}\right) - \left(\frac{31}{48}\right)x^2. \tag{20}$$

### 2.3 The Monte Carlo Scheme

The present Monte Carlo scheme is based on the continuous slowing down approximation.

Let us adopt spherical coordinates $(r,\theta,\phi)$ and assume that a stream of mono-energetic electrons irradiates a solid target in the $+z$ direction.

The path-length distribution is assumed to follow a Poisson-type law. The step-length $\Delta l$ is then given by

$$\Delta l = -\lambda_{el}\ln(1 - rnd_1), \tag{21}$$

where $rnd_1$ is a random number uniformly distributed in the range [0,1] and $\lambda_{el} = 1/N\sigma_{el}$ is the elastic mean free path calculated by using the Equations (11) and (12) (RPWEM, see refs. [1-3]). Note that here $N$ is the number of atoms per unit of volume in the target.

The energy loss $\Delta E$ along the segment of trajectory $\Delta l$ is approximated as follows

$$\Delta E = (dE/dl)\Delta l, \tag{22}$$

where $dE/dl$ is the Ashley's stopping power [4] calculated by Equations (19) and (20).

The polar scattering angle $\theta$ after an elastic collision is calculated assuming that the probability $P(\theta)$ of elastic scattering within an angular range from 0 to $\theta$ is a random number $rnd_2$ uniformly distributed in the range [0,1].

The azimuth angle $\phi$ can take on any value in the range [0, $2\pi$] selected by a random number $rnd_3$ uniformly distributed in that range.

Both $\theta$ and $\phi$ angles are calculated relative to the last direction in which the particle was moving before the impact.

The direction $\theta_z^{'}$ in which the particle is moving after the last deflection, relative to the $z$ direction, is given by

$$\cos\theta_z^{'} = \cos\theta_z \cos\theta + \sin\theta_z \sin\theta\cos\phi, \tag{23}$$

where $\theta_z$ is the angle relative to the $z$ direction before the impact.

The motion $\Delta z$ along the $z$ direction is then calculated by

$$\Delta z = \Delta l \cos\theta_z^{'}. \tag{24}$$

The new angle $\theta_z^{'}$ then becomes the incident angle $\theta_z$ for the next path length.

The particles are followed in their trajectories until their energies become lower than 50 eV or until they leave the solid target.

For surface films one has to take into account the interface between the film and the substrate. After crossing the interface, the changes in the scattering probabilities per unit length in passing from the film to the substrate and vice versa have indeed to be considered.

Let us denote with $p_1$ and $p_2$ the scattering probabilities per unit length for the two materials, where $p_1$ refers to the material in which the last elastic collision occurred and $p_2$ to the other one. Let us indicate with $d$ the distance, along the scattering direction, between the initial scattering and the interface.

If $rnd$ is a random number uniformly distributed in the range [0,1], the step-length $\Delta l$ is given by

$$\Delta l = \begin{cases} (1/p_1)[-\ln(1-rnd)] \\ for\ 0 \le rnd < 1-\exp(-p_1 d) \\ d + (1/p_2)[-\ln(1-rnd) - p_1 d] \\ for\ 1-\exp(-p_1 d) \le rnd \le 1 \end{cases}. \tag{25}$$

The energy loss $\Delta E$ is approximated by utilizing the same random number $rnd$ used to calculate $\Delta l$:

$$\Delta E = \begin{cases} (dE/dl)_1 (1/p_1)[-\ln(1-rnd)] \\ for\ 0 \le rnd < 1-\exp(-p_1 d) \\ (dE/dl)_1 d + (dE/dl)_2 (1/p_2)[-\ln(1-rnd) - p_1 d] \\ for\ 1-\exp(-p_1 d) \le rnd \le 1 \end{cases}, \tag{26}$$

where $(dE/dl)_1$ is the stopping power in the material where the last elastic collision occurred and $(dE/dl)_2$ the stopping power in the other material.

### 2.3.1 Sampling the scattering angle

For low atomic number elements (lower than ~30) and for some oxides, the differential elastic scattering cross-section can be safely approximated by the following function:

$$\frac{d\sigma}{d\Omega} = \frac{\Phi}{\left(1-\cos\theta+\Gamma\right)^2}, \tag{27}$$

where the quantities $\Phi$ and $\Gamma$ have to be determined in order to obtain the best fit of the total and the first transport elastic scattering cross-section previously calculated by using the RPWEM.

Let us now show how to calculate $\Phi$ and $\Gamma$ by the use of our knowledge of the total elastic scattering cross-section $\sigma_{tot}$ and of the first transport elastic scattering cross-section $\sigma_{tr}$ mentioned above (see Eqs. (12) and (13)). Note that, from Eq. (12), it follows that

$$\sigma_{el} = \frac{4\pi\Phi}{\Gamma\left(\Gamma+2\right)}, \tag{28}$$

so that the differential elastic scattering cross-section can be rewritten as

$$\frac{d\sigma}{d\Omega} = \frac{\sigma_{el}}{4\pi}\frac{\Gamma\left(\Gamma+2\right)}{\left(1-\cos\theta+\Gamma\right)^2}, \tag{29}$$

It is now easy to obtain the ratio $\Xi$ between the transport and the total elastic scattering cross-sections:

$$\Xi \equiv \frac{\sigma_{tr}}{\sigma_{el}} = \Gamma\left[\frac{\Gamma+2}{2}\ln\left(\frac{\Gamma+2}{\Gamma}\right)-1\right]. \tag{30}$$

The values of the total cross-section $\sigma_{tot}$ and the transport cross-section $\sigma_{tr}$ have to be numerically determined by using the RPWEM. In such a way it is possible to find their ratio $\Xi$ as a function, for any given target, of the electron kinetic energy *E*. The values of the screening parameter $\Gamma$ can be subsequently computed, by use of the knowledge of $\Xi$, by utilizing a bisection algorithm.

## 3 RESULTS AND DISCUSSION

The backscattering coefficient is defined as the fraction of electrons of the primary beam that emerge from the surface of an electron-irradiated target. Secondary electrons are not included in the definition of the backscattering coefficient: the energy cut-off is typically 50 eV.

The backscattering coefficient of electrons in bulk targets has been studied both experimentally and theoretically. Some investigators have suggested, on the basis of experimental evidences, that the absorption coefficient should approach 0 and the backscattering coefficient should approach 1, as the energy approaches 0 [5].

In Fig. 1 we show the trend of the backscattering coefficient as a function of the electron beam primary energy for electrons impinging on bulk targets of C, Al, and Cu as calculated by a Monte Carlo code. For the examined elements, the backscattering coefficient increases as the energy becomes lower than ~3000-4000 eV and decreases towards 1000 eV.

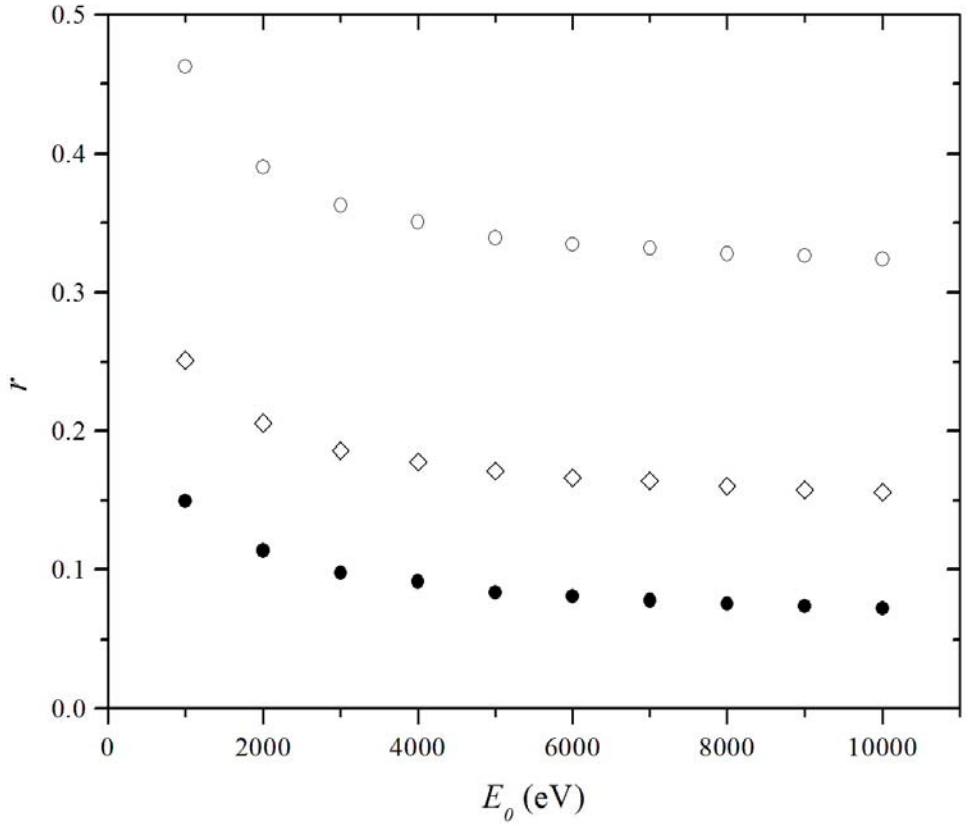


**Figure 1. Monte Carlo simulation of the backscattering coefficient *r* as a function of the primary energy $E_0$ for electrons impinging on bulk targets of C (bullets), Al (diamonds), and Cu (circles).**

The Monte Carlo code was then utilized to study the backscattering coefficient of supported thin films. The thickness of the substrate is assumed to be greater than the maximum range of penetration: in other words the substrate is considered as a bulk for the electron primary energies considered.

Investigating the behavior of the backscattering coefficient as a function of the primary energy for various film thicknesses, it can be noted the appearance, for carbon film thicknesses higher than ~100 Å, of relative maxima of absorption (and relative minima of backscattering). These features are presented, for three thicknesses (400, 600, and 800 Å) of C films deposited on Al and Cu substrates, in Figs. 2 and 3.

For low energies the curves follow the behavior of the backscattering coefficient of C, while for high energies they follow the behavior of the backscattering of the substrate. The backscattering coefficient reaches, as a consequence, a relative minimum and then it increases up to the substrate backscattering coefficient. Then it follows the trend of the backscattering coefficient of the substrate.

Another interesting characteristic of the relative minima is that their position shifts towards higher energies as the film thickness increases. This is quite reasonable because the backscattering coefficient of the system should approach the behavior of the backscattering coefficient of the substrate for very thin films and, on the other hand, approaches the energy dependence of the backscattering coefficient of C for thick films. So, as the film thickness increases, the positions of the relative minima shift towards higher energies while the peaks are broadening. The behavior of the energy position of the relative minima as a function of the film thickness is presented in Fig. 4 for Al substrate and in Fig. 5 for Cu substrate.

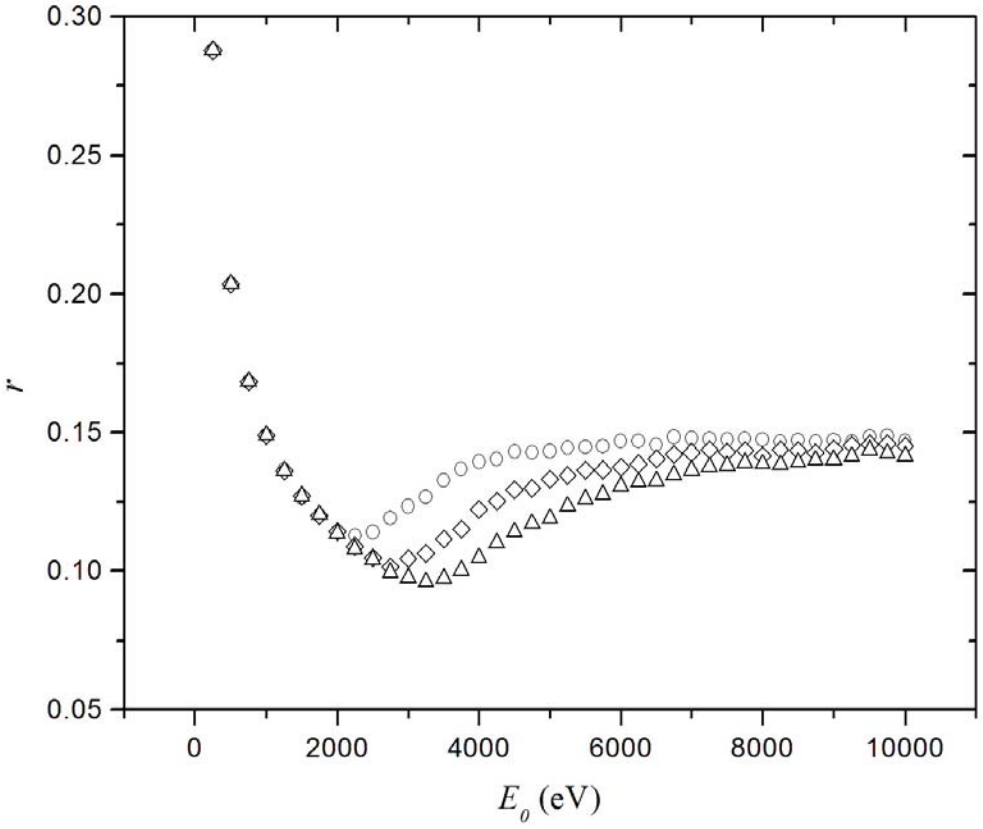


**Figure 2. Monte Carlo simulation of the electron backscattering coefficient r for C films deposited on Al substrates as a function of the beam primary energy $E_0$. C film thickness: 400 Å (circles), 600 Å (diamonds), and 800 Å (triangles).**

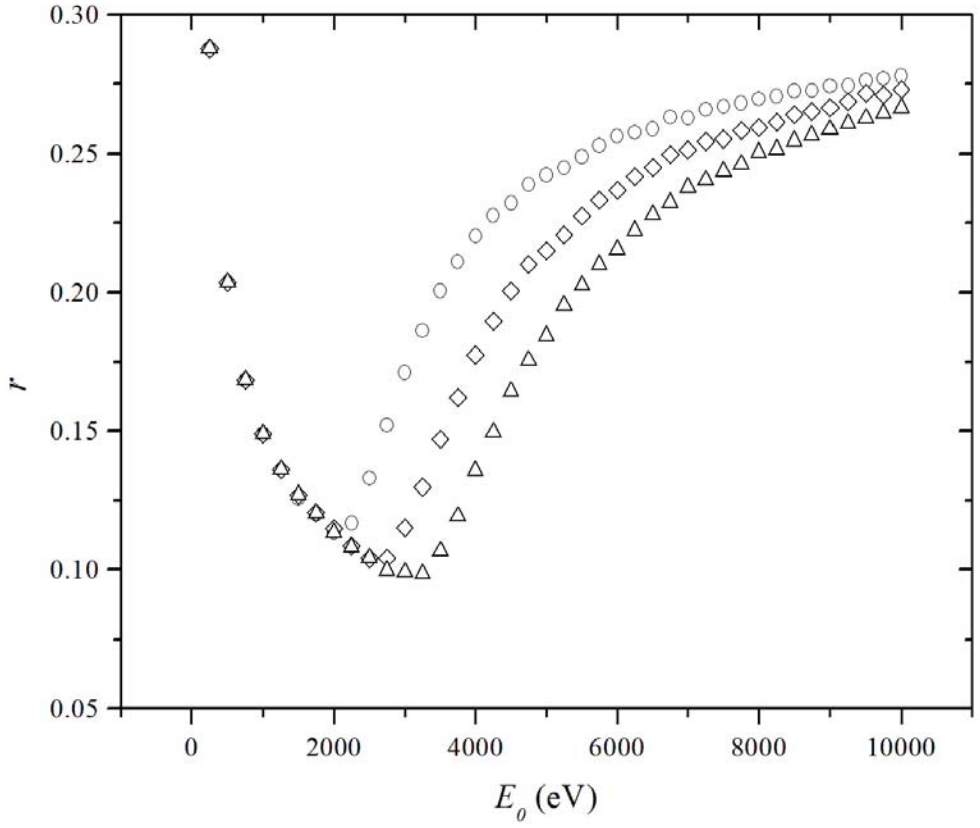


**Figure 3. Monte Carlo simulation of the electron backscattering coefficient *r* for C films deposited on Cu substrates as a function of the beam primary energy $E_0$. C film thickness: 400 Å (circles), 600 Å (diamonds), and 800 Å (triangles).**

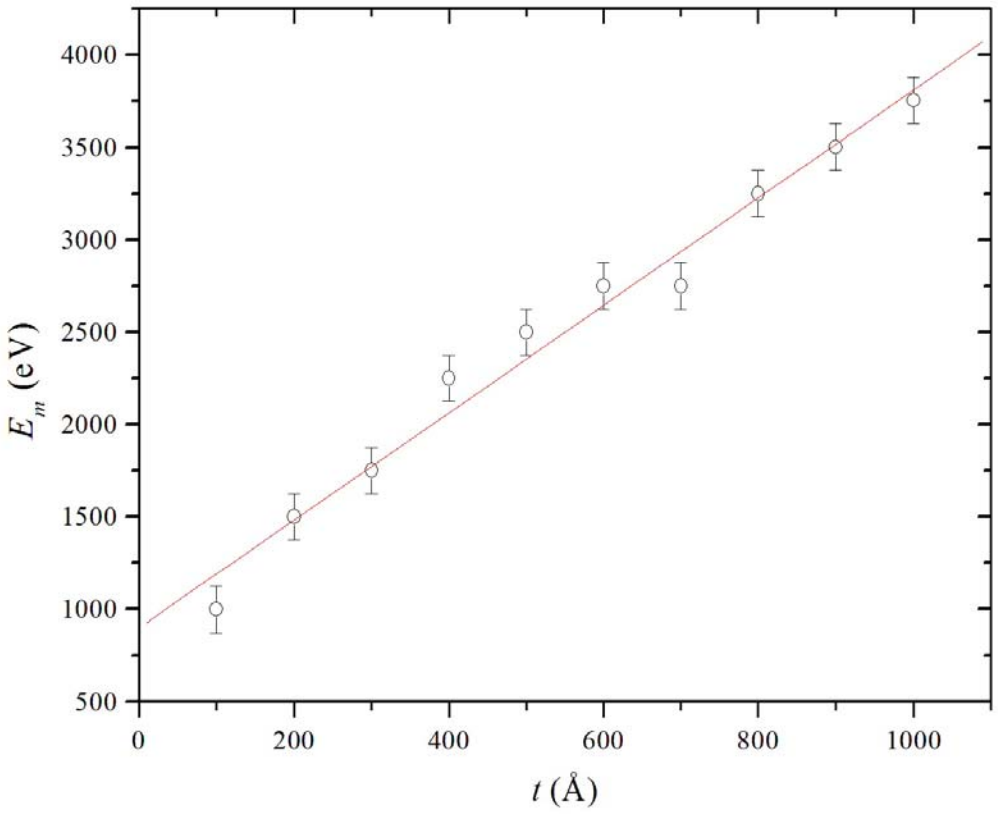


**Figure 4. Energy $E_m$ of the relative minimum of the backscattering coefficient as a function of the film thickness $t$ for C films deposited on Al substrates. Circles with the error bars represent the calculated data. The line is the best linear fit: $E_m=a\,t+b$ where $a$=2.9±0.1, $b$=900±90.**

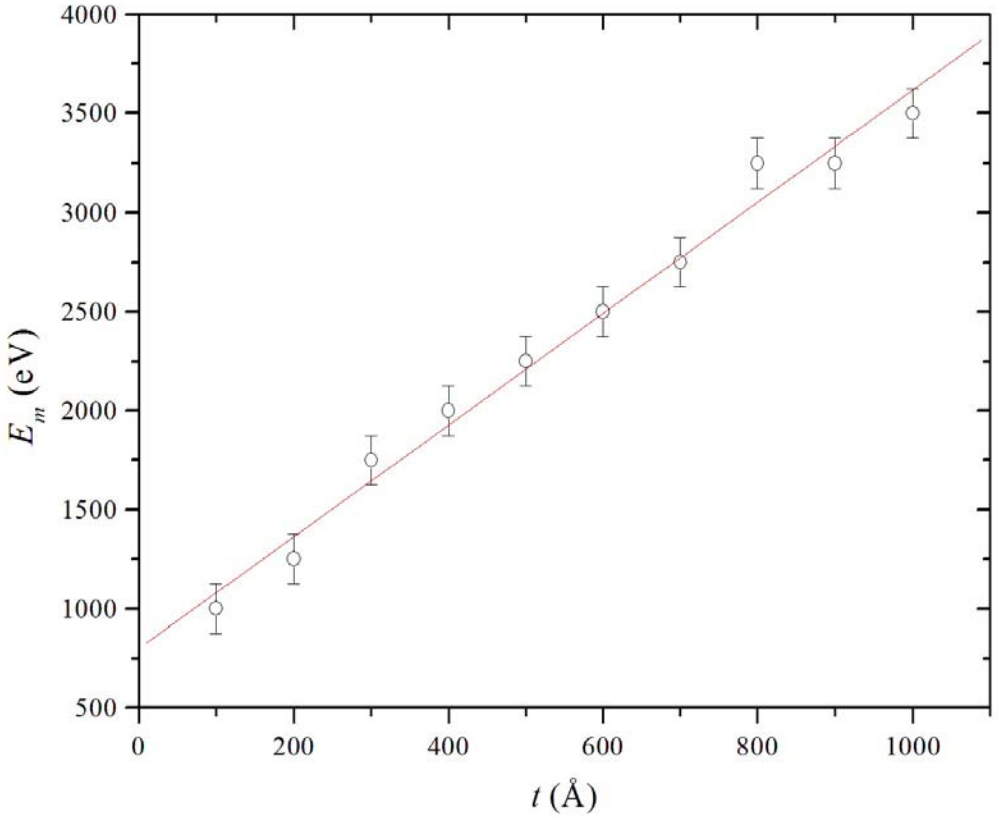


**Figure 5. Energy $E_m$ of the relative minimum of the backscattering coefficient as a function of the film thickness $t$ for C films deposited on Cu substrates. Circles with the error bars represent the calculated data. The line is the best linear fit: $E_m=a\,t+b$ where $a$=2.8±0.1, $b$=800±75.**

The curves in Figs. 4 and 5 show that the energy positions $E_m$ of the minima are independent on the substrate atomic number (see also Figs. 2, 3). This result is also quite reasonable: indeed we expect that the position of the relative minima is mainly related to the properties of penetration of the electrons in the supported film rather than in the substrate: the film represents, indeed, a barrier for the penetration in the substrate and, as a consequence, backscattering is more influenced by the film than the substrate, especially for low primary energies. If experimentally confirmed and quantitatively better defined, the qualitative trends presented in the paper can be used as a way to measure the carbon film thickness by a set of measures of the backscattering coefficient.

## 4 CONCLUSION

The study of C film is important for many applications. Carbon films deposited on polymeric substrates can be used to replace the metallic coatings on plastic materials used for food package. Carbon films are also widely employed in medical devices. This paper reports the results of a

Monte Carlo simulation of the backscattering coefficient of low--medium energy electron beams (from 250 eV to 10,000 eV) of C films of various thicknesses deposited on Al and Cu substrates. The aim of the paper was to investigate the behavior of the backscattering coefficient as a function of the beam primary energy and of the film thickness. The trends presented can be used to calculate the carbon film thickness by measuring the backscattering coefficient.

## 5 REFERENCES

1. M. Dapor, Electron-Beam Interactions with Solids. Application of the Monte Carlo Method to Electron Scattering Problems, Springer, Berlin (2003).

2. A. Jablonski, F. Salvat, C.J. Powell, "Comparison of Electron Elastic-Scattering Cross Sections Calculated from Two Commonly Used Atomic Potentials", *J. Phys. Chem. Ref. Data*, **33**, pp.409-451 (2004).

3. M. Dapor, "Elastic Scattering Calculations for Electrons and Positrons in Solid Targets", *J. Appl. Phys.*, **79**, pp.8406-8411 (1996).

4. J.C. Ashley, "Interaction of Low-Energy Electrons with Condensed Matter: Stopping Powers and Inelastic Mean Free Paths from Optical Data", *J. Electron Spectrosc. Relat. Phenom.*, **46**, pp.199-214 (1988).

5. R. Cimino, I.R. Collins, M.A. Furman, M. Pivi, F. Ruggiero, G. Rumolo, and F. Zimmermann, "Can Low-Energy Electrons Affect High-Energy Physics Accelerators?", *Phys. Rev. Lett.*, **93**, pp.01481-01484 (2004).